JGR Biogeosciences

RESEARCH ARTICLE
10.1029/2021JG006308

Carbon Emissions From the Edge of the Greenland Ice Sheet Reveal Subglacial Processes of Methane and Carbon Dioxide Turnover

Jesper R. Christiansen[1], Thomas Röckmann[2], Maria E. Popa[2], Celia J. Sapart[3,4], and Christian J. Jørgensen[5]

[1]Department of Geoscience and Natural Resource Management, University of Copenhagen, Copenhagen, Denmark, [2]Institute for Marine and Atmospheric Research Utrecht, Utrecht University, Utrecht, The Netherlands, [3]Labotorie de Glaciologie, Libre Université de Bruxelles, Bruxelles, Belgium, [4]Now at CO2 Value Europe, Bruxelles, Belgium, [5]Department of Bioscience, Arctic Environment, Aarhus University, Roskilde, Denmark

Key Points:

- Elevated methane (CH_4; average 19–71 ppm) and carbon dioxide (CO_2; average 476–521 ppm) in subglacial air indicate potentially high emissions from the ice sheet
- The isotopic signature of subglacial CH_4 indicate a microbial source of mixed origin from acetate fermentation and carbonate reduction
- Isotopic signatures of subglacial gCO_2 indicate that both methane oxidation and remineralization are likely subglacial sources of CO_2

Supporting Information:

Supporting Information may be found in the online version of this article.

Correspondence to:

J. R. Christiansen,
jrc@ign.ku.dk

Citation:

Christiansen, J. R., Röckmann, T., Popa, M. E., Sapart, C. J., & Jørgensen, C. J. (2021). Carbon emissions from the edge of the Greenland Ice Sheet reveal subglacial processes of methane and carbon dioxide turnover. *Journal of Geophysical Research: Biogeosciences*, *126*, e2021JG006308. https://doi.org/10.1029/2021JG006308

Received 27 FEB 2021
Accepted 3 NOV 2021

Author Contributions:

Conceptualization: Jesper R. Christiansen, Celia J. Sapart, Christian J. Jørgensen
Data curation: Jesper R. Christiansen, Thomas Röckmann, Maria E. Popa, Christian J. Jørgensen
Funding acquisition: Jesper R. Christiansen, Christian J. Jørgensen
Investigation: Jesper R. Christiansen, Christian J. Jørgensen
Methodology: Jesper R. Christiansen, Christian J. Jørgensen
Project Administration: Jesper R. Christiansen
Writing – original draft: Jesper R. Christiansen, Thomas Röckmann, Maria E. Popa, Celia J. Sapart, Christian J. Jørgensen

Abstract Direct gaseous emissions of methane (CH_4) and carbon dioxide (CO_2) from the subglacial environment under Greenland Ice Sheet (GrIS) were only recently discovered and it is yet to be determined how important it is for the panarctic carbon budget. We measured in situ net gaseous emissions of subglacial CH_4 and CO_2, dissolved concentrations and isotopic composition of gases (^{13}C and ^{2}H) at the onset, near maximum, and at the end of the melt season in 2018 and 2019. We found a tight relation between gaseous and dissolved CH_4 and CO_2, respectively, indicating that degassing from the subglacial meltwater is the main source of these gases in the subglacial air. The diurnal variability of in situ mole fractions of CH_4 and CO_2 in subglacial air was related to meltwater runoff showing that the net emission magnitude is directly related to glacial hydrology. We observed that maximum in situ mole fractions of CH_4 and CO_2 appeared at the onset of the melt season and decreased over the melt season. The isotopic signature of CH_4 in the subglacial air indicated that it likely originated from microbial methanogenesis which remained constant during the season. Isotopic signatures of subglacial CO_2 indicate mixed sources from microbial oxidation of CH_4, remineralization of sedimentary organic carbon, and possibly influenced by removal of CO_2 by weathering. Our study indicate large emissions of both CO_2 and CH_4, but continuous studies over entire melt seasons are needed to determine the origin and emission magnitudes and their relation to the glacial dynamics.

Plain Language Summary Wetlands and thawing permafrost are considered to be the primary sources of natural methane and carbon dioxide emissions in the Arctic. However, new discoveries show that these gases are also emitted in large quantities from the meltwater coming from under the Greenland Ice sheet. So far, subglacial gas emissions have only been investigated at two sites in Greenland and it is not known how much gas is released, where it comes from and how sensitive the emissions are to future climate change. The aim of our research was to investigate how much is emitted to the atmosphere and what the likely origin of these gases are. Our field measurements showed that the levels of methane in the glacial outlet cavity are up 100 times higher than the background levels of methane (two parts per million) in the atmosphere. Our results show that these gases originate from biological processes under the ice, and that the release rate is controlled by the melting of the glacier. Our study reveals new insight into this unknown Arctic source of greenhouse gases which will help us to understand its broader relevance for the atmospheric composition and its feedback to climate change.

1. Introduction

Ice sheets and glaciers separate large parts of the Earth's rocky surface and sediment deposits from the atmosphere. Until recently it was perceived that glaciated areas had no significant impact on the global carbon cycle and that only little carbon was exchanged across this icy barrier. Weathering of comminuted glacial bedrock consumes CO_2 and potentially makes glacial systems net sinks of atmospheric CO_2 (Graly et al., 2017; St Pierre et al., 2019). Recent field studies have found evidence for net emissions of both methane (CH_4) and carbon dioxide (CO_2) to the atmosphere from subglacial environments (Burns et al., 2018; Christiansen & Jørgensen, 2018; Lamarche-Gagnon et al., 2019; Pain et al., 2021) with estimates

of subglacial CH_4 emissions from the Leverett glacier draining the Greenland Ice sheet (GrIS; ~8 mmol CH_4 m^{-2} day^{-1}) being well within the range of major world rivers (range 0.01–500 mmol CH_4 m^{-2} day^{-1}; Lamarche-Gagnon et al., 2019). This shows that our understanding of the carbon balance of glaciers and ice sheets is incomplete.

Elevated concentrations and biological production of CH_4 in subglacial waters and sediments have been found under glaciers and ice sheets across Canada (Hamilton et al., 2013), Antarctica (Michaud et al., 2017; Stibal et al., 2012), West Greenland (Dieser et al., 2014), Iceland (Burns et al., 2018), and at the center of the GrIS (Christner et al., 2012; Souchez et al., 1995). Once formed under the ice, the CH_4 may either be stored as dissolved gas in the basal meltwater or accumulate as hydrates under high pressure (i.e., solid CH_4 bound in a crystal structure with water molecules; Wadham et al., 2012) both of which eventually will be exported to the proglacial zone via meltwater rivers and emitted to the atmosphere. Microbial potential to oxidize subglacial biological CH_4 to CO_2 has also been documented in sediment and water samples from below the GrIS and Antarctica (Dieser et al., 2014; Michaud et al., 2017). Subglacial meltwaters from central and south GrIS glaciers show consistently elevated dCO2 concentrations above atmospheric equilibrium with carbon isotopic signatures consistent with organic matter remineralization (Pain et al., 2021). These findings point to the potential occurrence of widespread subglacial biological processes responsible for production of CH_4 and CO_2 that can be emitted to the atmosphere. Organic carbon reserves in overridden paleosoils (Kohler et al., 2017) or marine sediments (Wadham et al., 2012) represents a large pool of substrate for these gases. Collectively, this indicates that conversion of subglacial organic carbon reserves may be more widespread and could represent a larger and more consistent net source of subglacial CH_4 and CO_2 to the atmosphere than previously assumed.

The very limited empirical evidence from field studies on subglacial CH_4 and CO_2 turnover processes and emissions (Burns et al., 2018; Christiansen & Jørgensen, 2018; Lamarche-Gagnon et al., 2019) is insufficient for understanding of the importance of subglacial carbon conversion for the atmospheric CO_2 and CH_4 composition and whether it can be regarded as potential climate amplifier (Wadham et al., 2008, 2019). In this article we present a new findings from field work carried out in the summers of 2018 and 2019 adding to fill our knowledge gap on subglacial carbon emission rates and turnover processes. We performed in situ high frequency measurements of the mole fractions of CH_4 and CO_2 in the subglacial air inside the air-filled ice cavities found at the ice edge, and collected discrete gas and water samples for analyses of the isotopic composition of CH_4 and CO_2. The aims were to (a) measure the magnitude of subglacial carbon fluxes to the atmosphere at the onset, near maximum, and late stages of the melt season, (b) to study the diurnal and seasonal temporal dynamics of subglacial CO_2 and CH_4 emissions and their relationship with glacial hydrology, and (c) to investigate the potential sources of subglacial CH_4 and CO_2.

2. Materials and Methods

2.1. Site Description

The study site is located at an elevation of 450 m above sea level at a lateral subglacial meltwater outlet on the southern flank at the terminus of the Isunnguata Sermia Glacier at the western margin of the GrIS (67°09′16.40″N 50°04′08.48″W). According to Rennermalm et al. (2013) the catchment of the studied lateral outlet is 70 km^2 and represents a site that to a large degree is impacted by marginal processes and less representative for the larger catchments of major glaciers in the area (Isunnguata, Russell, and Leverett).

The area in front of the meltwater outlet consists of abraded granodioritic gneiss bedrock with large boulders and patches of gravel, sand, and silt deposited by meltwater. The glacier front contained highly irregular cracks and air-filled cavities, which changed over the season as the ice melted and deformed (Figure 1).

The landscape in the Kangerlussuaq area is typical of west Greenland, where numerous, narrow and up to 600 m deep valleys are oriented in a East-West direction. These valleys extend below the ice sheet, and subglacial valleys can in places reach depths of hundreds of meters below sea level. Deglaciation and re-advance of the GrIS in this region during the Holocene has resulted in buried subglacial carbon rich sediments that were once exposed (Kellerman et al., 2020; Kohler et al., 2017). In the proglacial zone of the study area continuous permafrost extends at places up to 350 m below the surface (Drake et al., 2017), but the

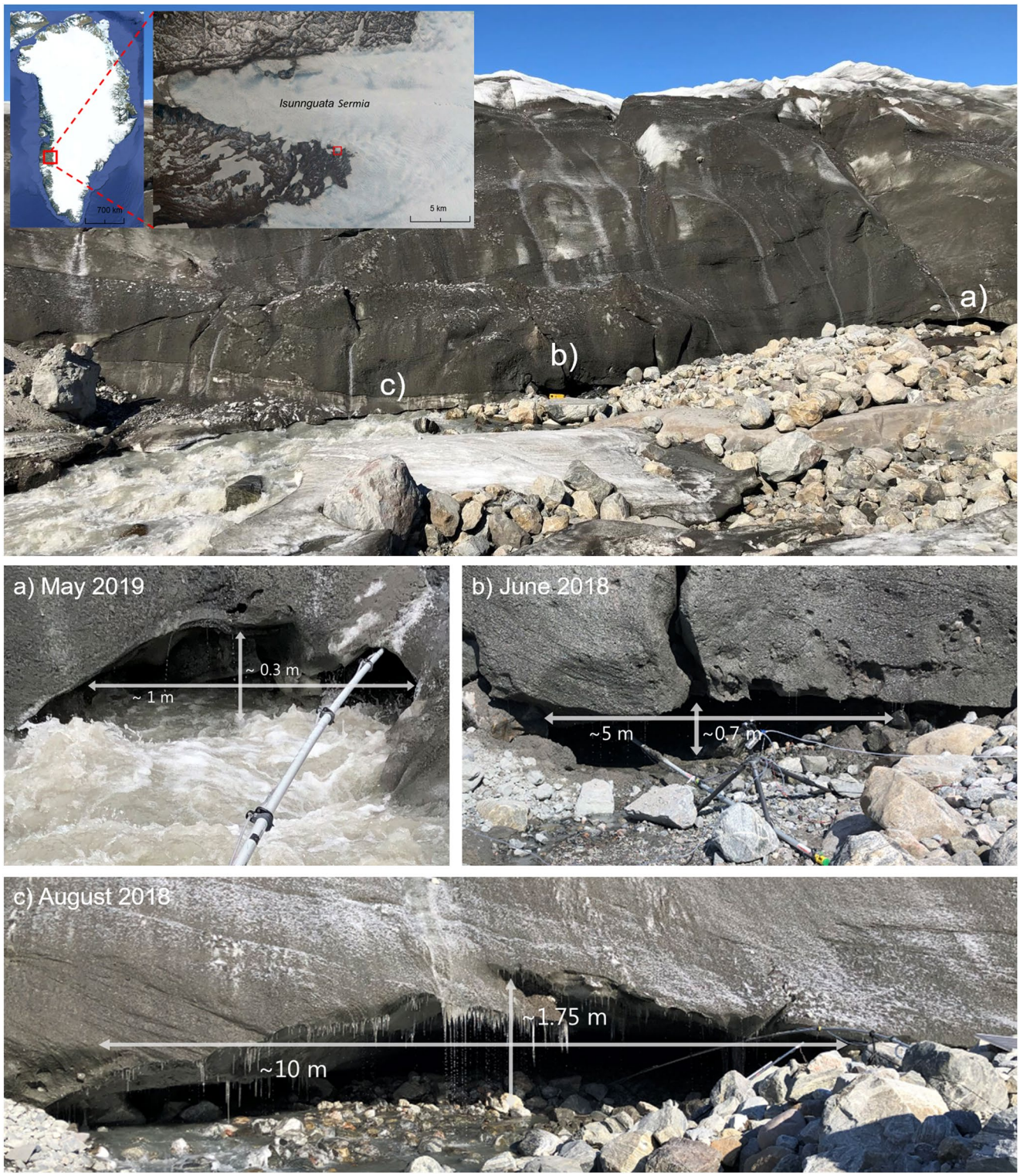

Figure 1. Top panel: Map of West Greenland and Isunnguata glacier with study site indicated at red squares (top left inset) and an overview of the study site at the ice front in June 2018. Letters (a, b, and c) indicate location of measurement of mole fractions of CH_4 and CO_2 in subglacial air and sampling of melt water at three different stages during the melt season. (a) May 2019 represents the early stage meltwater discharge where the meltwater openings are small and mostly filled with water. (b) June 2018 represents a progressive stage of opening where multiple cracks and caves are air filled after the meltwater has carved out channels in the ice. (c) August 2018 represents the mature stage of evolution of the meltwater channel, where the volume of the outlet is at its maximum and most of it is air filled due to decreasing meltwater volumes.

Isunnguata glacier and GrIS in this area is warm based with an annual ice flow of 150–200 m and surface meltwater reaching the base of the glacier (Graly et al., 2014).

We sampled melt water and gas at a lateral subglacial outlet to the Isunnguata Sermia glacier draining the GrIS in West Greenland (Figure 1, top panel). The sampling was done during three campaigns covering the periods May 3–6, 2019, June 18–28, 2018, and August 16–24, 2018, during which the cross-sectional area of the subglacial outlet changed size and position along the ice edge (Figures 1a–1c). These periods are assumed to represent the early, middle, and late stages of a typical melt season.

2.2. Measurements of Subglacial Air Velocity, Temperature, Humidity, Atmospheric Pressure, and Water Level

At the end of an aluminum pole that extended under the ice for retrieval of unmixed subglacial air we attached instrumentation to measure subglacial air velocity (hot-wire anemometer, model 313-T-DCI-F900-L-O, Onset Computer Corporation, Bourne, MA, USA), temperature and humidity (model 313-S-THB-M008, Onset Computer Corporation). The anemometer was positioned so it measured the wind movement perpendicular to the cross section. Atmospheric pressure was measured outside the cave (model 313-S-BPB-CM50, Onset Computer Corporation). The data were recorded on a HOBO datalogger (model U30-NRC-VIA-05-S100-000, Onset Computer Corporation) at 10 s intervals. These measurements were conducted during the June and August campaigns only. We were only able to measure the air velocity for a short period in June as the sensor was damaged by water spray in the ice cave.

During the August 2018 campaign, we also installed an underwater pressure transducer (Onset Computer Corporation) in the outlet stream to estimate the temporal variability of the water level. Air pressure from the meteorological station was used as the atmospheric reference needed to calculate the water level above the pressure transducer. The water level was assumed as a proxy for melt water runoff, but the discharge volume was not estimated.

2.3. Measurements of Gaseous Subglacial CH_4 and CO_2 Mole Fractions and Flux Calculation

Dry mole fractions of CH_4 and CO_2 in the subglacial air were measured with a portable $CH_4/CO_2/H_2O$ analyzer (Ultraportable Greenhouse Gas Analyzer (UGGA), ABB – Los Gatos Research, San Jose, CA, USA) powered by a 12 V 100 Ah LiFePO4 battery. Due to shifting positions and geometries of the subglacial cave, the gas sampling setup with the UGGA was not identical during all campaigns, but generally followed the same procedure (Figures 1a–1c). The cross-sectional areas of the outlet during the three campaigns were estimated based on field observations of the dimensions (height and width) of the opening (Figures 1a–1c). Gas measurements were performed by attaching a tube to a 9 m aluminum pole and sampling the air inside the subglacial cavities (Figures 1a–1c). A water trap fixed to the end of the aluminum pole ensured a liquid free air stream to the gas analyzer.

2.4. Collection of Discrete Water and Gas Samples

Water and gas samples were taken at three different locations after the subglacial water and air had mixed to different degrees with the ambient environment. For the air samples, the simultaneous variations in mole fraction and isotopic composition were used to determine the isotopic composition of the source ($\delta^{13}C\text{-}CH_4$, $\delta^{2}H\text{-}CH_4$, and $\delta^{13}C\text{-}CO_2$) of the subglacial CH_4 and CO_2 using the Keeling plot approach. This is a widely used method to determine the isotope composition of unknown sources of CO_2 or CH_4 in situations where CH_4 or CO_2 from a source (in our case the subglacial environment) is added to a constant background (atmosphere; Pataki et al., 2003).

Water and gas were sampled twice per day, in the morning and evening, assumed to represent low and high water flow derived from the water level measurements. Samples were gathered during the periods of June 22–26, 2018 and August, 19–22, 2018, respectively.

Air samples were collected in 2L gas tight aluminum foil bags (Supel™-Inert Multi-Layer Foil, Sigma-Aldrich, St. Louis, MO, USA) which were filled by a small diaphragm pump. We sampled gas from three

locations (Figures 1a–1c); inside the ice cave, representing the least mixed subglacial air we could possibly sample (minimal mixing with atmosphere), right outside the ice cave (subglacial air mixed with atmospheric air) and 2 km from the ice edge (background atmosphere, no subglacial air signal).

For practical reasons the water was sampled at slightly different positions than the gas. Thus, the first water sample representing the subglacial water was sampled right where the meltwater exits the ice (PW1), the second sample (PW2) 200 m downstream and the third sample was taken at the same position as the third gas sample, 2 km away from the ice edge (PW3). Unfiltered water was sampled in 120 mL glass bottles with butyl rubber septa and tightened with aluminum screw caps. The bottles were rinsed three times with melt water and filled under water ensuring that no bubbles were included. Immediately after sampling, 12 µL saturated $HgCl_2$ solution was added to the bottles to exclude further biological activity (Magen et al., 2014). Water was sampled in duplicates, one sample for measurement of dissolved CH_4 and another for measurement of CH_4 isotopic composition.

Gas and water samples were stored cold and dark until analysis, except during transport from Greenland to Denmark where samples were transported in the cargo hold of the airplane. Transport resulted in loss of three gas samples, but water samples remained intact. Upon arrival in Denmark the gas bags were immediately sent to Utrecht over land. In Utrecht, the samples in the bags were first analyzed for CH_4 isotopes by directly extracting sample from the bag, and then transferred to glass flasks for storage until the CO_2 isotope analysis were possible. We used 1 L flasks from Normag, Ilmenau, with PCTFE sealing, that were shown to be stable for CO_2 (Rothe et al., 2005). The flasks were pre-conditioned and evacuated. The transfer was done by connecting the bag to the flask, evacuating the connection to avoid admixing of room air, and then opening both the bag and the flask valves. The total time from sampling in the field to transfer was up to 14 days.

2.5. Dissolved CH_4 Concentrations

The dissolved CH_4 was extracted at room temperature (23°C) using headspace mixing and the concentration was calculated according to the method outlined in Magen et al. (2014). Shortly, 10 mL of water (V_{HS}) was replaced with CH_4 free N_2 gas and the headspace was afterward pressurized to 2 atm (P_{HS}), by adding another 10 mL N_2 amounting to 20 mL of gas in the headspace (V_{gas}). The sample was then thoroughly stirred on a shaking table with 150 rpm for 3 min. A 5 mL gas sample was retrieved by syringe from the headspace and transferred to a factory evacuated 3 mL Exetainer with a butyl rubber screw cap (Labco, Lampeter, UK). The evacuation efficiency was accepted when the plunger from the 5 mL syringe changed by visibly dropped by 2–2.5 mL after insertion through the septum indicating an adequately evacuated vial. We used factory evacuated vials. Non-evacuated vials and samples were discarded ensuring that only properly evacuated vials were used. The pressurization of the Exetainer was done to facilitate subsequent gas chromatography analysis by an autosampler using similar prepared triplicate gas standards in the same types of vials. The CH_4 mole fraction in the headspace (CH_4,mf) of extracted gas samples was determined on a gas chromatograph equipped with an FID detector. CH_4 was separated on a HayeSep Q column heated to 60°C, with pure N_2 5.0 as carrier gas. Using a 5-point calibration curve the headspace CH_4 mole fraction in ppm was determined. The total dissolved CH_4 was calculated as the sum of the headspace CH_4 and CH_4 still dissolved in the water after shaking (Magen et al., 2014). The ideal gas law was used (laboratory temperature at extraction was 23°C) to convert the headspace concentration to gas amount (mole; Equation 1). The dissolved CH_4 in the remaining 110 mL water was calculated by multiplying the Bunsen coefficient for 23°C (0.03273) at 0 salinity (assumed as we have no data) with the amount of headspace CH_4 to calculate the remaining dissolved CH_4 in water (Yamamoto et al., 1976), accounting for the ratio of water and gas volume (Magen et al., 2014; Equation 2). It is assumed that the dissolved CH_4 we estimate here represent the in situ amount, as samples were kept in bottles without headspace and sterilized to avoid microbial CH_4 oxidation.

$$CH_{4,HS} = CH_{4,mf} * V_{HS} * \frac{P_{HS}}{R * T_{HS}} \left[\mu mol\ L^{-1}\right] \quad (1)$$

$$\mathrm{CH}_{4,\mathrm{water}} = \beta * \frac{\mathrm{CH}_{4,\mathrm{conc}} * V_{\mathrm{gas}} * \left(V_{\mathrm{water}} / V_{\mathrm{HS}}\right)}{R * T_{\mathrm{water}}} \left[\mu mol\ L^{-1}\right] \quad (2)$$

where $CH_{4,conc}$ is the headspace CH_4 mole fraction in ppm, V_{HS} is the headspace volume in L, P_{HS} is the headspace pressure in atm, R is the gas constant (atm L K^{-1} mol^{-1}), T_{HS} is the headspace temperature in °K, β is the Bunsen coefficient, V_{gas} is the total volume of gas in headspace in L, V_{water} is the water volume after replacement in L, and T_{water} is the water temperature (similar to T_{HS}).

2.6. Dissolved CO_2 Concentrations

Dissolved CO_2 in meltwater was measured in situ using an eosGP2 probe (Eosense Inc., Dartmouth, Canada) connected to a Campbell CR1000 datalogger (Campbell Scientific Inc., Logan, UT, USA) during the June 2018 campaign. The eosGP2 probe works by passive diffusion allowing dissolved CO_2 to diffuse through a membrane in to a cavity, where it is analyzed for CO_2 in gaseous form and reports a value in ppm. The cavity inside the eosGP equilibrates at around 90 s with the water. We set the sampling interval to 10 s and dissolved CO_2 concentrations given in ppm. A custom calibration for measurements at CO_2 concentrations close to the atmospheric equilibrium had been done prior to the field work by Eosense. Before each deployment, we let the eosGP2 probe equilibrate with the atmospheric background CO_2 concentration for ~1 hr to monitor possible drift and/or sensitivity of the response of the CO_2 signal when switching the probe between the aqueous and gaseous phases. At deployment the eosGP2 probes were fixed in place and the diffusion membrane initially placed 15 cm below the surface of the meltwater at low flow conditions.

2.7. Isotopic Analyses of Gas and Water Samples

The isotopic composition of CH_4 ($\delta^{13}C$-CH_4 and $\delta^{2}H$-CH_4) was measured using continuous-flow isotope ratio mass spectrometry (CF-IRMS) on a ThermoFinnigan Delta^{plus} XL isotope ratio mass spectrometer. The air samples were injected via a mass flow controller into the sample loop of the extraction system and further processed and analyzed as described in Röckmann et al. (2016). The CH_4 in the water samples was extracted with a headspace mixing method and further analyzed on the same analytical system, as described in Jacques et al. (2020). Further information on the data processing is available in Brass and Röeckmann (2010) and Sapart et al. (2011). Specifically, the CH_4 isotopic data were corrected to account for system variability and non-linearity effects and reported in ‰ versus VPDB for $\delta^{13}C$ values and ‰ versus VSMOW for $\delta^{2}H$ values. The measurement reproducibility was calculated from the standard deviation of reference air injections.

The isotopic composition of CO_2 ($\delta^{13}C$ and $\delta^{18}O$) was analyzed with the CF-IRMS system described in Naus et al. (2018) and Pathirana et al. (2015). This system is primarily meant for CO isotopes, but can also analyze CO_2 isotopes is small samples (~2 mL air at normal atmospheric mole fractions). In short, the CO_2 is cryogenically separated from the air, further purified chromatographically, and then injected into the IRMS via an open split inlet. The results are related to the VPDB and VSMOW scales via a reference air cylinder with known isotopic composition. The typical precision, estimated as repeatability of multiple measurements of a constant gas (Target cylinder), is about 3 ppm for the CO_2 mole fractions, and 0.05‰ and 0.14‰ for $\delta^{13}C$ and $\delta^{18}O$, respectively.

3. Results and Discussion

3.1. Subglacial CH_4 and CO_2 Mole Fractions and Concentrations in Air and Meltwater

Figure 2 shows measured mole fractions of gaseous CH_4 (gCH_4) and CO_2 (gCO_2) (Figures 2a–2c) and concentrations of dissolved CH_4 (dCH_4) (Figures 2d–2f) for the three campaigns. During all campaigns the gCH_4 and gCO_2 mole fractions measured at the outlet were continuously and significantly elevated compared to the ambient mole fractions of these gases (Figures 2a–2c). Also in the water, dCH_4 concentrations are strongly elevated compared to the saturation concentration of CH_4 (0.02 μmol L^{-1}) in contact with ambient air (Figures 2d–2f). Collectively, this clearly demonstrates that a source for these gases exists below the ice sheet.

Concentrations of dCH_4 were highest close to the outlet and decreased strongly with distance from the outlet. Degassing is assumed to be the main loss process for dCH_4 from the meltwater between the sampling points PW1 and PW3 (Christiansen & Jørgensen, 2018). Oxidation of dCH_4 to CO_2 can contribute as well,

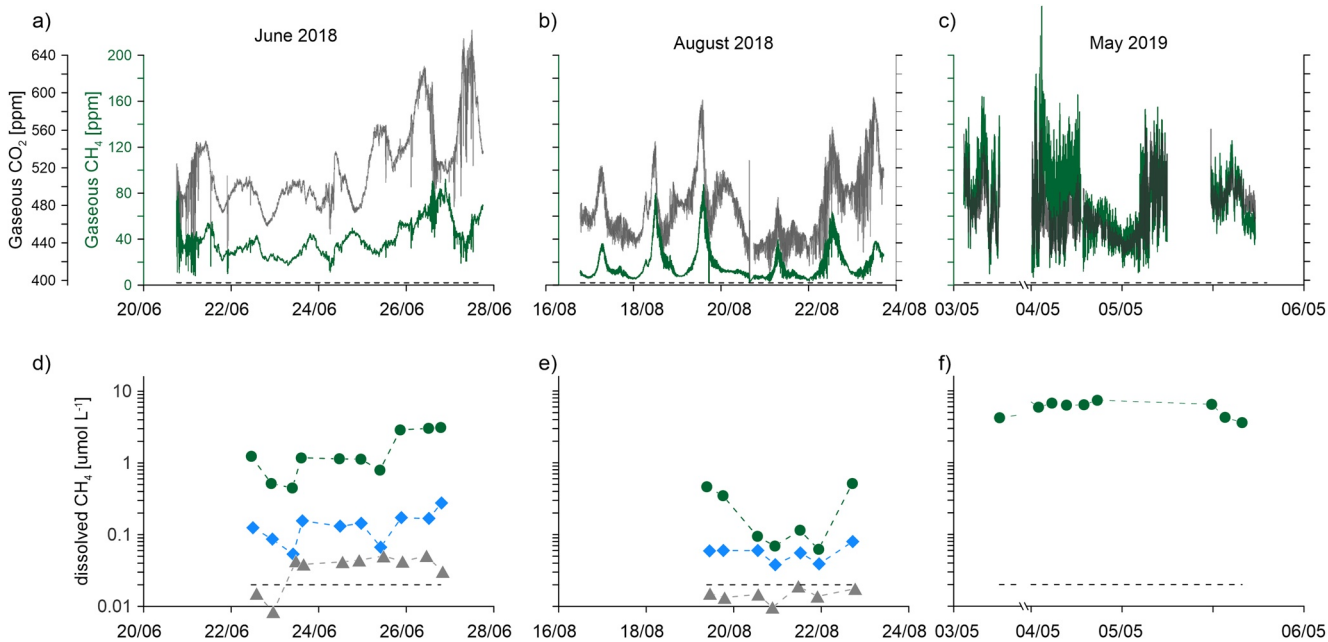

Figure 2. Upper panels: Time series of subglacial gaseous CH_4 (green) and CO_2 (gray) mole fractions in (a) June 2018, (b) August 2018, and (c) May 2019. Black dashed line indicates the atmospheric mole fractions of CH_4 (2 ppm) and CO_2 (400 ppm) measured on site. Lower panels: Dissolved CH_4 concentrations at three distances (● PW1: 0 m from outlet; ◆ PW2: 200 m from the outlet; ▲ PW3: 2,000 m from the outlet) for (d) June 2018, (e) August 2018, and (f) May 2019. Black dashed line indicates the estimated dissolved concentration of CH_4 at atmospheric equilibrium (0.02 μmol L^{-1}). For interpretation of colors the reader is referred to the online publication.

but oxidation rates measured previously are low (Dieser et al., 2014), indicating that it cannot be the main cause for the observed decrease here. The dCH_4 at PW3 occasionally is lower than the atmospheric equilibrium during the June and August 2018 campaigns, but it is not possible to determine if it is attributed to the inherent uncertainty of dCH_4 determination or in-stream oxidation of CH_4 (Figures 2d and 2e).

In the June and August campaigns both CH_4 and CO_2 showed diurnal variability with some inconsistency between the gases, which indicate that several factors contribute to this observed variability (Figures 2a–2c).

In June 2018, the temporal behavior of gCH_4 and gCO_2 were related to variations in melt water and maximum mole fractions of both gases generally occurred at low flow conditions. A possible explanation is that during the period of low water flow less surface water purges the subglacial environment, increasing the degassing rate of dCH_4 and dCO_2 from the relative enriched meltwater increasing the mole fractions of CH_4 and CO_2 in subglacial cavities which is then transported to the opening and emitted. Additionally, the increase of melting during the day will dilute the CH_4 and CO_2 bearing subglacial meltwater resulting in lower degassing and hence lower mole fractions in the subglacial air at high water flow. The control of degassing on gCH_4 and gCO_2 mole fractions is supported by simultaneous measurements of gCO_2 and dCO_2 in the June campaign (Figure S2a in Supporting Information S1) and water level for a single diurnal cycle. These measurements showed identical temporal variability of dCO_2 and gCO_2, with maximum dCO_2 and gCO_2 occurring at low flow and higher dCO_2 concentrations relative to gCO_2 (Figure S2 in Supporting Information S1) strongly suggesting that the meltwater is the source of gCO_2.

In the August 2018 campaign the diurnal pattern of gCH_4 and partly that of gCO_2 were slightly different than observed in June 2018 and anti-correlated to the flow variations observed in the melt water river in August (Figure S1 in Supporting Information S1), with maximum gCH_4 and gCO_2 arriving at the outlet on average 6 hr after minimum flow (Figure S1 in Supporting Information S1). At this waning stage of the melt season the internal drainage system has reached its maximum volume, which may not be entirely water filled because of lower melt rates. This could potentially leave air filled subglacial caves where CH_4 and CO_2 can accumulate during low flux and the release to the atmosphere occurs more slowly due to slower transport of the subglacial air compared to the melt water. In the early stage of the melt season, where the

Table 1
Average, Minimum, and Maximum Gaseous Subglacial CH_4 and CO_2 Mixing Ratios in May 2019, June 2018, and August 2018 Campaigns

	CH_4 mole fraction (ppm)				CO_2 mole fraction (ppm)			
	Average	Min	Max	*x*Atmosphere[a]	Average	Min	Max	*x*Atmosphere[a]
May 2019	70.8	6.67	243	35.4	476	425	580	1.2
June 2018	40.4	8.06	92.1	20.2	521	426	667	1.3
August 2018	18.6	3.68	87.5	9.3	479	397	596	1.2

[a]The enrichment factor (*x*Atmosphere) relative to the atmospheric background for CH_4 and CO_2 is based on in situ measurements of the atmospheric mole Fractions of CH_4 = 2 ppm and CO_2 = 400 ppm.

drainage system volume is smaller and mostly filled with water, most degassing more likely occurs closer to the outlet. In the May 2019 campaign, where no visible caves had developed at the edge (representing the early melt season) diurnal variability was difficult to discern.

Both the level and the temporal variability of gCH_4 mole fractions were different between the seasons, with the highest average and maximum measured in May 2019, followed by June 2018 and the lowest average mole fractions in August 2018 (Figures 2a–2c and Table 1). The average enrichment factor (gCH_4/atmospheric CH_4) decreased from May to August from 35 to 9 (Table 1). For gCO_2 there was less difference between the seasons and the average enrichment factor was 1.2–1.3 (Table 1). It was previously estimated that the subglacial air velocity could reach up to 2 m s^{-1} (Christiansen & Jørgensen, 2018) and in this study we observed fluctuations of the wind speed in this range from 0.1 to 2.5 m s^{-1} (Figure S3 in Supporting Information S1) with an average speed of 0.8 m s^{-1} and a standard deviation of 0.28 m s^{-1}. However, we only obtained wind speed measurements for part of the June 2018 campaign and not for the other campaigns, making emission calculations too speculative. Improving the measurement of the subglacial air velocity is key for quantification of gaseous flux estimates in the future.

The short-term (minute scale) variability of gCH_4 and gCO_2 was apparently influenced by turbulent mixing with the more dilute atmosphere outside the cave. This was indicated during all campaigns by rapidly fluctuating gCH_4 and gCO_2 mole fractions (Figures 2a–2c) and increasing air temperature and decreasing humidity of the subglacial air (Figure S3 in Supporting Information S1). However, for most of the time, the relative humidity in the cave remained at 100% and air temperatures were low (below 0.5°C) whereas the outside temperatures were higher (diel variation between 1°C and 12°C) indicating an overall low degree of mixing. In particular, the longer-scale diurnal variability is likely not caused by mixing with the outside atmosphere, but by the subglacial supply of trace gases. This is supported by the fact that in August 2018 the subglacial air temperature varied in a pattern that corresponded to the diurnal variation in melt water flow, with highest subglacial air temperatures observed under maximum flow (Figure S3 in Supporting Information S1). Whether the higher subglacial air temperature is caused by heat dissipation from frictional heating of the turbulent meltwater or higher influx of relatively warmer surface water is unknown. However, we conclude that the short-term variability of CO_2 and CH_4 mole fractions in the subglacial cave system is a direct product of occasional turbulent mixing at the interface between the ice cave and the atmosphere, whereas the diurnal cycle of gCH_4 and gCO_2 and total net emission we observe (Figures 2a–2c) is directly related to the flow of melt water and not the atmospheric conditions outside the cave.

3.2. Isotopic Composition of Subglacial CH_4 and CO_2

Figure 3 shows a dual isotope plot of the isotopic signatures ($\delta^{13}C$-CH_4 and $\delta^{2}H$-CH_4) estimated from separated Keeling plots (Figures S4a–S4d in Supporting Information S1), for gaseous CH_4 and the isotopic composition of the dissolved CH_4 compared to measurements of $\delta^{13}C$ and $\delta^{2}H$ values of discrete gas samples for ambient air. These estimates clearly indicate that dCH_4 and gCH_4 originate from microbial CH_4 production, most likely from acetate fermentation, but possibly also mixed with CH_4 originating from hydrogenotrophic methanogenesis as has been suggested in earlier studies (Lamarche-Gagnon et al., 2019).

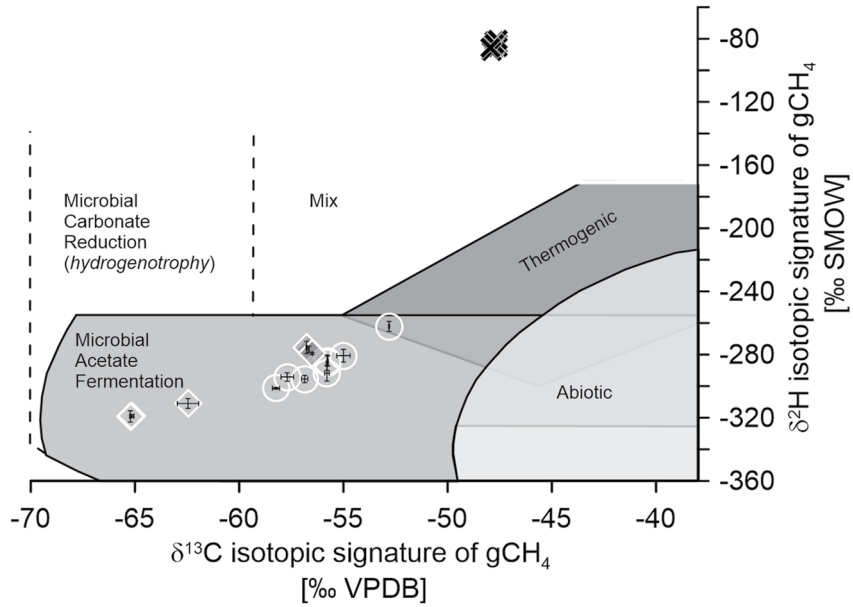

Figure 3. Dual isotope plot of Keeling plot estimates of the isotope source signatures (δ^{13}C-CH_4 and δ^2H-CH_4) for gCH_4 (transparent symbols and white marker line) in June 2018 (circles) and August 2018 (diamonds). Standard errors of the estimate of isotopic signature (gCH_4) are shown as error bars. Isotopic composition (δ^{13}C-CH_4 and δ^2H-CH_4) of dCH_4 are shown in white symbols with black edge for June 2018 (circles) and August 2018 (diamonds) campaigns. Gray shaded areas modified after Whiticar (1999). For comparison, the δ^{13}C and δ^2H values of atmospheric CH_4 are shown with *X*'s.

The δ^{13}C values of dCH_4 at PW1 were depleted compared to the atmosphere and varied little during each campaign and between June and August campaigns, suggesting a similar source over the melt season. The isotopic signature of gCH_4 was slightly enriched in both ^{13}C and ^{2}H and more variable compared to δ^{13}C values for dCH_4 for most of the June and August (Figure 3 and Figure S4 in Supporting Information S1).

The isotopic signatures (δ^{13}C and δ^2H) of gCH_4 varied along a line (slopes ≈ 5 and 7.4 for June and August 2018 campaigns, respectively), that resembles an oxidation pattern (Figure 3) suggesting in situ transformation of the subglacial CH_4. This points to the presence of an active biological system below the ice, but its importance for modifying CH_4 emission to the atmosphere is still unknown. The slope is smaller than what has earlier been attributed to oxidation of dCH_4 (a = 8.6–9; Burns et al., 2018; Etiope & Sherwood Lollar, 2013) and while this indicates that oxidation of subglacial CH_4 takes place, the lower slope for gCH_4 we find suggests additional isotope fractionation processes could impact the isotopic signature of gCH_4. Future research will focus on understanding what drives the deviation between the isotopic signature of gCH_4 and dCH_4 as it has implications for interpretation of the origin of subglacial CH_4.

Further evidence of an active microbial transformation of the subglacial CH_4 and CO_2 emissions is provided by the relationship between isotopic δ^{13}C signatures of dissolved and gaseous subglacial CH_4 and of gaseous subglacial CO_2 (Figures 4a and 4b). The difference (−6‰ to 22‰) between the δ^{13}C isotopic signatures of gCO_2 and gCH_4, suggests that a substantial proportion of the subglacial gCO_2 is derived from CH_4 oxidation in the subglacial environment (Whiticar, 1999). Using the Keeling plot approach for δ^{13}C of gCO_2 (Figure S5 in Supporting Information S1) shows that the samples group in the zone of CH_4 oxidation on the dual isotope plot (Figure 4b). This provides field experimental confirmation for subglacial CH_4 oxidation to CO_2 which in previous studies has only been inferred indirectly (Burns et al., 2018).

We also observed that less δ^{13}C-depleted gCO_2 corresponded to increasing gCO_2 mole fractions (Figure 4a). This cannot be explained by the subglacial CO_2 originating only from CH_4 oxidation, which produces ^{13}C-depleted CO_2 and indicates that one or more additional and isotopically heavier sources of CO_2 contribute to subglacial CO_2. Mixing of subglacial air with isotopically heavier atmospheric CO_2 could in principle

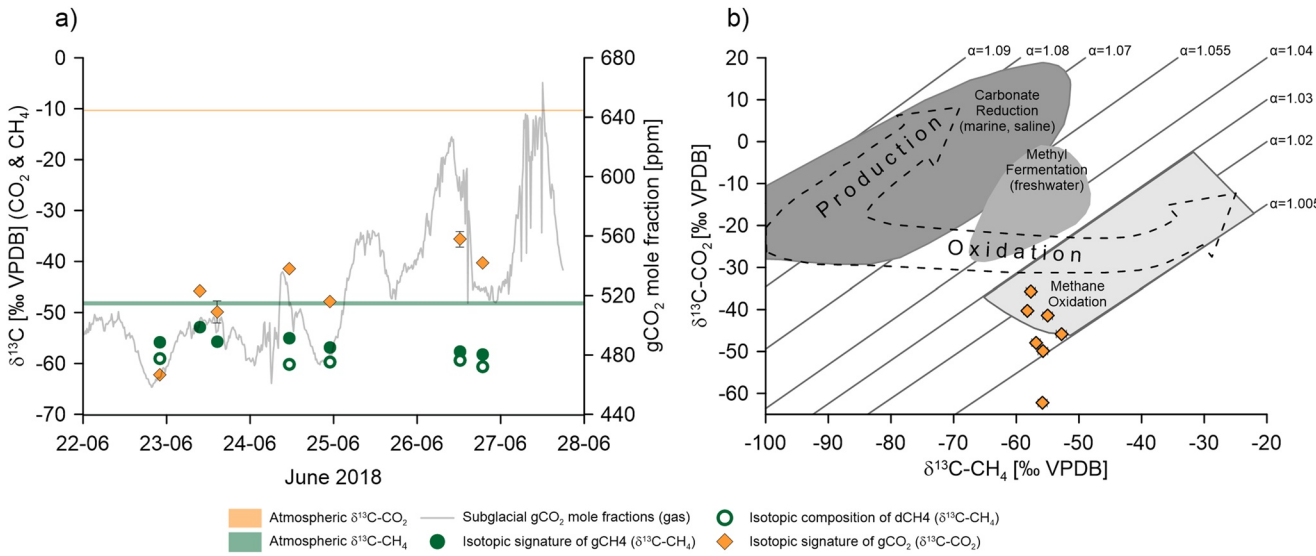

Figure 4. (a) Temporal variation of isotopic ($\delta^{13}C$) source signatures for gaseous CO_2 and CH_4 and the isotopic composition of dissolved subglacial CH_4. Subglacial gaseous CO_2 mole fractions (ppm) are superimposed as gray line. (b) Dual isotope plots showing the resulting Keeling plot isotope signature of gCO_2 ($\delta^{13}C$-CO_2) plotted against the isotopic signature of gCH_4 (orange diamonds). Standard errors of the Keeling plot intercept are shown as vertical and horizontal error bars. In most cases error bars were smaller than the symbols. Shaded areas in panel (b) are adapted from Whiticar, 1999. For interpretation of colors the reader is referred to the online publication.

enrich the gCO_2 in ^{13}C (as we observed for $\delta^{13}C$-CH_4), but it cannot increase gCO_2 mole fractions above the ambient level (Figures 2a–2c).

Instead, it is possible that the increasing mole fraction and ^{13}C-enrichment of gCO_2 could be due to an increased proportion of gCO_2 (and dCO_2) originating from remineralized subglacial organic carbon (Pain et al., 2021), as the export of dCO_2 from remineralization of organic carbon in subglacial sediments must also be governed by melt flow and subsequent degassing into the subglacial air. Subglacial dissolved organic carbon at this outlet (Andrews et al., 2018), a possible substrate for both methanogenesis and remineralization, was more enriched ($\delta^{13}C$-DOC: −29.8‰ to −24‰) in ^{13}C than subglacial CH_4. Carbonate weathering likely contributes to dCO_2 in the meltwater at this site (Graly et al., 2014, 2017; Pain et al., 2021). However, the estimated depleted isotopic gCO_2 signature indicates that the inorganic C source is of lesser importance here as carbonates are relative much more enriched in ^{13}C than organic carbon and CH_4. This is consistent with (Graly et al., 2017; Pain et al., 2021) that shows that dCO_2 in the subglacial outlets in the study area can be dominated by organic carbon sources.

The possible multiple sources contributing to dCO_2/gCO_2 and the lack of data in our study makes the calculation of the partitioning of the contribution to dCO_2 from CH_4 oxidation and remineralization (and possibly from weathering of dissolved inorganic carbon (DIC) and uptake of atmospheric CO_2) speculative. Pain et al. (2021) used the most depleted $\delta^{13}C$-CH_4 values in meltwater to derive a conservative estimate of the CH_4-derived CO_2. However, this estimate may likely underestimate the contribution of CH_4 oxidation, if CH_4 oxidation happens during transport from source to sampling point because dCH_4 is then more enriched here than at the subglacial origin. dCH_4 sampled at the subglacial source would be ideal, but unfeasible. So clearly, more data is needed sampled at different times during the melt season to constrain the $\delta^{13}C$ isotopic signatures of subglacial CH_4, buried organic carbon and DIC which may all contribute to the observed isotopic signature of dCO_2 and gCO_2.

We observed increasing CO_2/CH_4 ratios in the subglacial air from average values between 5 and 10 in May 2019 to average values >80 in August 2018 (Figure S6 in Supporting Information S1). This shows that the export and emission of CO_2 changes during the melt season in a clear relationship to CH_4 (Figures 2a–2c and Table 1). This indicates a dynamic relationship between gCH_4/gCO_2, meaning that these two gases could largely originate from the same substrate, for example, CH_4 oxidation and/or remineralization of organic carbon. As the internal drainage system develops until maximum flow over the melt season, the residence

time of the subglacial melt water should increase when the melting decreases later in the year. This longer residence time could enhance subglacial CH_4 oxidation and its contribution to dCO_2, and limit the export and subsequent emission of subglacial CH_4 to the atmosphere. Also, the expanding ablation zone over the melt season connects pockets of subglacial sediment which could not only lead to increased mobilization of CH_4 (Lamarche-Gagnon et al., 2019; and hence oxidation), but also of remineralization of organic carbon to CO_2 (Kellerman et al., 2020; Kohler et al., 2017). Oxygen availability in the anoxic subglacial environment limits both the oxidation of subglacial CH_4 (Michaud et al., 2017) and remineralization. However, it is plausible that oxygen is supplied to subglacial environments, both from melting of O_2-containing basal ice or import of oxygenated surface melt water. We observed that the subglacial melt water at the outlet was fully oxygenated to nearly 100% of the atmospheric equilibrium during the June 2018 campaign (data not shown) indicating conditions conducive for both processes to occur in the subglacial environment at this site.

Several CO_2 generating processes likely occur simultaneously, and how they contribute to the resulting net emission in the proglacial zone is closely connected to the glacial hydrology and basal distribution of carbon containing sediment and bedrock of the catchment (Graly et al., 2017). The interaction between these factors complicates the interpretation of $\delta^{13}C$-CO_2 values and future research should focus on partitioning the subglacial CO_2 sources (oxidation, remineralization, dilution with atmospheric air, inorganic carbon) using both gCO_2 and dCO_2 together with measurements of subglacial CH_4. This source identification should enable us to narrow in on where in the subglacial system, in transit with the meltwater (Dieser et al., 2014; Lamarche-Gagnon et al., 2019) or at the ice-sediment interface at the subglacial source (Burns et al., 2018; Michaud et al., 2017) that the production and release of CO_2 happens.

It has to be noted that the studied outlet represents a smaller marginal catchment of the glacier which may contribute to a higher degree of basal oxygen input from meltwater than can be expected for larger catchments. This oxygenated basal environment could enhance biological CO_2 production relative to weathering. Hence, it remains to be studied if similar patterns of CO_2/CH_4 dynamics exist for outlets of larger glaciers draining GrIS as the contribution of chemical weathering to CO_2 dynamics may be substantial different (Graly et al., 2017).

4. Conclusions

In this study we present direct continuous measurements of gaseous evasion of CH_4 and CO_2 from below the GrIS at three different stages of a melt season indicating emissions of CH_4 and CO_2 from the subglacial environment to the atmosphere. These unique seasonal measurements are supported by isotopic studies of both subglacial CH_4 and CO_2 in discrete gas and water samples. Results show that degassing of dissolved gases happens both under the ice in the subglacial cave system and in the proglacial river system confined to a relatively narrow zone from the outlet.

Gaseous CH_4 and CO_2 emissions are closely linked to the glacial hydrology and emissions from the outlet increase over the melt season related to the discharge and development of the subglacial drainage system, allowing more degassing in the subglacial system later in the season. Considering that the phenomenon should also occur at other glaciers along the margin of GrIS and in Iceland, this topic warrants intensified research.

The isotopic signatures show that subglacial CH_4 originates from biological production of CH_4 by microbial methanogenesis in the suggested region for acetoclastic methanogenesis, but it cannot be ruled out that the CH_4 can also originate from hydrogenotrophic methanogenesis. The carbon source can likely be from buried organic carbon, which is the source throughout the melt season. Isotopic analysis also shows that the emitted subglacial CO_2 is linked to oxidation of this subglacial CH_4. However, the isotopic composition of subglacial CO_2 point to other possible sources of subglacial CO_2 apart from CH_4 oxidation and we suggest that remineralization of organic carbon most likely contributes to the emission of CO_2 at the outlet. It is possible that weathering in the subglacial meltwater moderates CO_2 dynamics as it is known from other glaciers. The proportion of CO_2 relative to CH_4 increases over the melt season possibly reflecting increased oxidation of CH_4 and remineralization of organic carbon. This is likely fueled by a combination of increased oxygen input from surface water and longer residence time of melt water in the subglacial drainage system. However, it is still unknown where in the subglacial system (sediment, melt water, or both) the CH_4

oxidation takes place. The interpretation of the isotope signals suggests that the emitted CH_4 and CO_2 undergo biogeochemical transformation below the ice and that mixing or dilution with other sources during transport under the ice can occur.

Our study shows that large amounts of biogenic CH_4 and CO_2 are emitted from a GrIS outlet glacier via glacial meltwater. However, considerable uncertainty still exists, related to the quantification of the exact mass flux of CH_4 and CO_2 due to an unknown partitioning between aqueous and gaseous fluxes, as well as uncertainty of the measurement of physical parameters (e.g., wind speed and direction) controlling the net emission. Furthermore, the studied lateral outlet only represents a minor catchment of the GrIS and similar investigations are needed for larger glacial outlets. Thus, there is a need to advance the fundamental knowledge of the emission of subglacial CO_2 and CH_4 and the biogeochemical processes governing the production and turnover of subglacial carbon to understand this unknown carbon-cryosphere feedback from glaciers and ice sheets worldwide and determine its importance for the atmospheric composition of CH_4 and CO_2.

Conflict of Interest

The authors declare no conflicts of interest relevant to this study.

Data Availability Statement

The data used in this study has been published and can be accessed online through University of Copenhagens Electronic Research Data Archive (ERDA) (at https://doi.org/10.17894/ucph.597b96ab-eef5-4be4-b4dd-b21998e2ed3b).

Acknowledgment
This study was kindly funded by Hartmann Fonden (Grant No. A32524).

References

Andrews, M. G., Jacobson, A. D., Osburn, M. R., & Flynn, T. M. (2018). Dissolved carbon dynamics in meltwaters from the Russell Glacier, Greenland Ice Sheet. *Journal of Geophysical Research: Biogeosciences*, *123*(9), 2922–2940. https://doi.org/10.1029/2018JG004458

Brass, M., & Röeckmann, T. (2010). Continuous-flow isotope ratio mass spectrometry method for carbon and hydrogen isotope measurements on atmospheric methane. *Atmospheric Measurement Techniques*, *3*, 1707–1721. https://doi.org/10.5194/amt-3-1707-2010

Burns, R., Wynn, P. M., Barker, P., McNamara, N., Oakley, S., Ostle, N., et al. (2018). Direct isotopic evidence of biogenic methane production and efflux from beneath a temperate glacier. *Scientific Reports*, *8*(1), 17118. https://doi.org/10.1038/s41598-018-35253-2

Christiansen, J. R., & Jørgensen, C. J. (2018). First observation of direct methane emission to the atmosphere from the subglacial domain of the Greenland Ice Sheet. *Scientific Reports*, *8*(1), 16623. https://doi.org/10.1038/s41598-018-35054-7

Christner, B. C., Montross, G. G., & Priscu, J. C. (2012). Dissolved gases in frozen basal water from the NGRIP borehole: Implications for biogeochemical processes beneath the Greenland Ice Sheet. *Polar Biology*, *35*(11), 1735–1741. https://doi.org/10.1007/s00300-012-1198-z

Dieser, M., Broemsen, E. L., Cameron, K. A, King, G. M., Achberger, A., Choquette, K., et al. (2014). Molecular and biogeochemical evidence for methane cycling beneath the western margin of the Greenland Ice Sheet. *The ISME Journal*, *8*(11), 2305–2316. https://doi.org/10.1038/ismej.2014.59

Drake, H., Suksi, J., Tullborg, E. L., & Lahaye, Y. (2017). Quaternary redox transitions in deep crystalline rock fractures at the western margin of the Greenland ice sheet. *Applied Geochemistry*, *76*, 196–209. https://doi.org/10.1016/j.apgeochem.2016.12.001

Etiope, G., & Sherwood Lollar, B. (2013). Abiotic methane on Earth. *Reviews of Geophysics*, *51*, 276–299. https://doi.org/10.1002/rog.20011

Graly, J. A., Drever, J. I., & Humphrey, N. F. (2017). Calculating the balance between atmospheric CO_2 drawdown and organic carbon oxidation in subglacial hydrochemical systems. *Global Biogeochemical Cycles*, *31*(4), 709–727. https://doi.org/10.1002/2016GB005425

Graly, J. A., Humphrey, N. F., Landowski, C. M., & Harper, J. T. (2014). Chemical weathering under the Greenland Ice Sheet. *Geology*, *42*(6), 551–554. https://doi.org/10.1130/G35370.1

Hamilton, T. L., Peters, J. W., Skidmore, M. L., & Boyd, E. S. (2013). Molecular evidence for an active endogenous microbiome beneath glacial ice. *The ISME Journal*, *7*(7), 1402–1412. https://doi.org/10.1038/ismej.2013.31

Jacques, C., Gkritzalis, T., Tison, J.-L., Hartley, T., van der Veen, C., Röckmann, T., et al. (2020). Carbon and hydrogen isotope signatures of dissolved methane in the Scheldt Estuary. *Estuaries and Coasts*, *44*, 137–146. https://doi.org/10.1007/s12237-020-00768-3

Kellerman, A. M., Hawkings, J. R., Wadham, J. L., Kohler, T. J., Stibal, M., Grater, E., et al. (2020). Glacier outflow dissolved organic matter as a window into seasonally changing carbon sources: Leverett Glacier, Greenland. *Journal of Geophysical Research: Biogeosciences*, *125*, 1–16. https://doi.org/10.1029/2019jg005161

Kohler, T. J., Žárský, J. D., Yde, J. C., Lamarche-Gagnon, G., Hawkings, J. R., Tedstone, A. J., et al. (2017). Carbon dating reveals a seasonal progression in the source of particulate organic carbon exported from the Greenland Ice Sheet. *Geophysical Research Letters*, *44*(12), 6209–6217. https://doi.org/10.1002/2017GL073219

Lamarche-Gagnon, G., Wadham, J. L., Sherwood Lollar, B., Arndt, S., Fietzek, P., Beaton, A. D., et al. (2019). Greenland melt drives continuous export of methane from the ice-sheet bed. *Nature*, *565*(7737), 73–77. https://doi.org/10.1038/s41586-018-0800-0

Magen, C., Lapham, L. L., Pohlman, J. W., Marshall, K., Bosman, S., Casso, M., & Chanton, J. P. (2014). A simple headspace equilibration method for measuring dissolved methane. *Limnology and Oceanography: Methods*, *12*(9), 637–650. https://doi.org/10.4319/lom.2014.12.637

Michaud, A. B., Dore, J. E., Achberger, A. M., Christner, B. C., Mitchell, A. C., Skidmore, M. L., et al. (2017). Microbial oxidation as a methane sink beneath the West Antarctic Ice Sheet. *Nature Geoscience*, *10*(8), 582–586. https://doi.org/10.1038/ngeo2992

Naus, S., Röckmann, T., & Popa, M. E. (2018). The isotopic composition of CO in vehicle exhaust. *Atmospheric Environment*, *177*, 132–142. https://doi.org/10.1016/j.atmosenv.2018.01.015

Pain, A. J., Martin, J. B., Martin, E. E., Rennermalm, Å. K., & Rahman, S. (2021). Heterogeneous CO_2 and CH_4 content of glacial meltwater from the Greenland Ice Sheet and implications for subglacial carbon processes. *The Cryosphere*, *15*(3), 1627–1644. https://doi.org/10.5194/tc-15-1627-2021

Pataki, D. E., Ehleringer, J. R., Flanagan, L. B., Yakir, D., Bowling, D. R., Still, C. J., et al. (2003). The application and interpretation of Keeling plots in terrestrial carbon cycle research. *Global Biogeochemical Cycles*, *17*(1). https://doi.org/10.1029/2001GB001850

Pathirana, S. L., van der Veen, C., Popa, M. E., & Röckmann, T. (2015). An analytical system for stable isotope analysis on carbon monoxide using continuous-flow isotope-ratio mass spectrometry. *Atmospheric Measurement Techniques*, *8*(12), 5315–5324. https://doi.org/10.5194/amt-8-5315-2015

Rennermalm, A. K., Smith, L. C., Chu, V. W., Box, J. E., Forster, R. R., Van den Broeke, M. R., et al. (2013). Evidence of meltwater retention within the Greenland ice sheet. *The Cryosphere*, *7*(5), 1433–1445. https://doi.org/10.5194/tc-7-1433-2013

Röckmann, T., Eyer, S., van der Veen, C., Popa, M. E., Tuzson, B., Monteil, G., et al. (2016). In situ observations of the isotopic composition of methane at the Cabauw tall tower site. *Atmospheric Chemistry and Physics*, *16*(16), 10469–10487. https://doi.org/10.5194/acp-16-10469-2016

Rothe, M., Jordan, A., & Brand, W. A. (2005). Trace gases, $\delta^{13}C$ and $\delta^{18}O$ of CO_2 in air samples: Storage in glass flasks using PCTFE seals and other effects. In D. Worthy, & L. Wuang (Eds.), *Proceedings of the 12th IAEA/WMO meeting of CO_2 experts* (pp. 64–70). WMO-GAW Report.

Sapart, C. J., van der Veen, C., Vigano, I., Brass, M., van de Wal, R. S. W., Bock, M., et al. (2011). Simultaneous stable isotope analysis of methane and nitrous oxide on ice core samples. *Atmospheric Measurement Techniques*, *4*(12), 2607–2618. https://doi.org/10.5194/amt-4-2607-2011

Souchez, R., Lemmens, M., & Chappellaz, J. (1995). Flow-induced mixing in the GRIP basal ice deduced from the CO_2 and CH_4 records. *Geophysical Research Letters*, *22*(1), 41–44. https://doi.org/10.1029/94GL02863

Stibal, M., Wadham, J. L., Lis, G. P., Telling, J., Pancost, R. D., Dubnick, A., et al. (2012). Methanogenic potential of Arctic and Antarctic subglacial environments with contrasting organic carbon sources. *Global Change Biology*, *18*(11), 3332–3345. https://doi.org/10.1111/j.1365-2486.2012.02763.x

St Pierre, K. A., St Louis, V. L., Schiff, S. L., Lehnherr, I., Dainard, P. G., Gardner, A. S., et al. (2019). Proglacial freshwaters are significant and previously unrecognized sinks of atmospheric CO_2. *Proceedings of the National Academy of Sciences of the United States of America*, *116*(36), 17690–17695. https://doi.org/10.1073/pnas.1904241116

Wadham, J. L., Arndt, S., Tulaczyk, S., Stibal, M., Tranter, M., Telling, J., et al. (2012). Potential methane reservoirs beneath Antarctica. *Nature*, *488*(7413), 633–637. https://doi.org/10.1038/nature11374

Wadham, J. L., Hawkings, J. R., Tarasov, L., Gregoire, L. J., Spencer, R. G. M., Gutjahr, M., et al. (2019). Ice sheets matter for the global carbon cycle. *Nature Communications*, *10*(1), 3567. https://doi.org/10.1038/s41467-019-11394-4

Wadham, J. L., Tranter, M., Tulaczyk, S., & Sharp, M. (2008). Subglacial methanogenesis: A potential climatic amplifier? *Global Biogeochemical Cycles*, *22*(2). https://doi.org/10.1029/2007GB002951

Whiticar, M. J. (1999). Carbon and hydrogen isotope systematics of bacterial formation and oxidation of methane. *Chemical Geology*, *161*(1–3), 291–314. https://doi.org/10.1016/S0009-2541(99)00092-3

Yamamoto, S., Alcauskas, J. B., & Crozier, T. E. (1976). Solubility of methane in distilled water and seawater. *Journal of Chemical & Engineering Data*, *21*(1), 78–80. https://doi.org/10.1021/je60068a029